Modeling of the effect of the beta phase deformation on the alpha phase precipitation in near-beta titanium alloys

Julien da Costa Teixeira, Benoît Appolaire, Elisabeth Aeby-Gautier, Sabine Denis, Fabien Bruneseaux

Modeling of the effect of the β phase deformation on the α phase precipitation in near-β titanium alloys

Julien Da Costa Teixeira [a,b], Benoît Appolaire [a,1], Elisabeth Aeby-Gautier [a], Sabine Denis [a], Fabien Bruneseaux [a]

[a] *LSG2M, École des Mines de Nancy, Parc de Saurupt, 54042 Nancy Cedex, France*

[b] *Snecma, 171 Bd de Valmy - BP31, 92702 Colombes Cedex, France*

Abstract

A model has been developed in order to describe the influence of a prior plastic deformation of the β phase above the transus on the precipitation of the α phase occurring during a subsequent cooling. The model relies on the calculation of the nucleation and growth rates of the α precipitates at the grain boundaries, based on a model presented formerly. Two major modifications have been carried out: first, the geometrical representation of the β microstructure accounts for subgrains resulting from the deformation process; second, the calculation of the nucleation rate is dependent on the conditions of the plastic deformation. A careful analysis of the main parameters of the model has led to distinguish between several assumptions: the Widmanstätten colonies are likely to cross the subgrains during their growth; and the critical width of the transition from the allotriomorphs to the Widmanstätten plates is likely to decrease when the misorientation angle of the grain boundary decreases. Calculations performed for assessing the influence of the strain and strain rate on the transformation kinetics are in good agreement with previous measurements.

Key words: titanium alloys, simulation, nucleation, kinetics, plastic deformation

[1] Corresponding author. Fax: (33) (0)3 83 58 40 56.
e-mail: benoit.appolaire@mines.inpl-nancy.fr

Article published in Acta Materialia 54 (2006) 4261–4271

1 Introduction

The optimization of the thermo-mechanical treatments applied to titanium alloys relies on the prediction of the microstructure evolutions (grain growth, recrystallization or phase transformation) occurring during the different steps of the process (e.g. forging, cooling or aging). The key point for the modeling of the whole process is to predict how the microstructure resulting from one operation will affect the microstructure evolutions during the subsequent one. In this paper, we present a model able to predict the influence of a plastic deformation of the β phase above the transus on the precipitation of the α phase during a subsequent cooling. Indeed, it is well known that the mechanisms involved, and by the way the final microstructure as well as the transformation rate are greatly influenced by the parameters of a prior plastic deformation [1,2]. In a deformed β microstructure, the morphologies of the α phase which appear at the grain boundaries are favored to the detriment of the intragranular morphologies. It has been shown experimentally that this feature comes mainly from an increase of the nucleation sites density, as well as from an increase of the nucleation rate. These observations point out the two main issues which have to be dealt with for a quantitative modeling of the process: (i) the model must include an explicit calculation of the nucleation and growth rates of the α precipitates at the grain boundaries. (ii) Moreover, it is necessary to know the grain boundary density and, to this aim, to identify relevant geometrical parameters of the deformed β microstructure (e.g. grain size), as well as their dependence on the plastic deformation conditions.

In this study, the first issue is treated by adapting a model relying on the calculation of the nucleation and growth rates of the grain boundary precipitates [3]. The second issue could be inspired by former models developed for the case of steels [4,5], for which a prior plastic deformation of the austenite shows similar effects on the ferrite precipitation [4,6–9]. Nevertheless, this analogy should be considered with care, because the microstructural evolutions in β occurring during a plastic deformation are very different from those in austenite. Thus, for the case of titanium alloys, a specific analysis is proposed here.

2 Model

2.1 Geometrical assumptions and overall transformation rate

2.1.1 Undeformed state

In the titanium alloys studied, the morphologies formed at high temperatures are allotriomorph precipitates wetting the grain boundaries, and Widmanstätten plates colonies growing from α_{GB} as shown in Fig. 1. These morphologies will be called α_{GB} and α_{WGB} respectively. In our model, the microstructure morphologies and their evolutions have been simplified as follows.

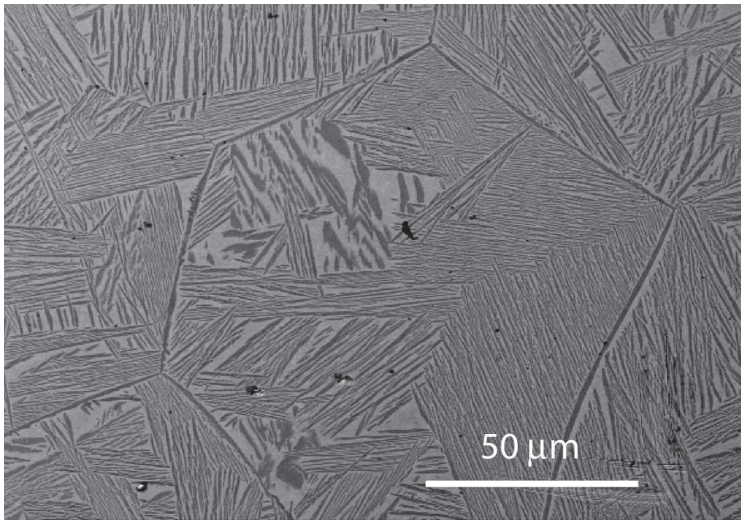

Fig. 1. SEM micrograph showing typical morphologies of the α phase in a near β titanium alloy.

(i) The solution treatment above the β transus causes the growth of large β grains ("initial" grains) with almost the same size ($\approx 100\,\mu$m diameter). In order to simplify the calculations, these grains are represented by equivalent spheres with a specific surface very close to that of the real grains, and one diameter D_{gr} for all grains, depending only on the temperature and duration of the solution treatment. The surface of the spheres is divided into 14 equal surfaces with area $S_{\mathrm{face}} = \pi\, D_{\mathrm{gr}}^2/14$, to mimic the grain boundaries (GBs), which are mostly high angle GBs.
(iii) During the cooling, the progression of the phase transformation follows the sequence shown in Fig. 2, following [3]: α_{GB} allotriomorphs nucleate on GBs until complete covering. The resulting α_{GB} layers are assumed to follow a diffusion controlled planar growth. Then, colonies of α_{WGB} appear on α_{GB}, and grow inside the initial β grains.

The progression of the transformation is calculated inside a representative

volume embedding 100 initial β grains. Each of them is treated independently, i.e. the growing α precipitates cannot cross the initial β GBs to interact with the precipitates in neighbouring grains. At each time step, the width of α_{GB}, the length of the α_{WGB} colonies, the number of α_{WGB} colonies per initial β grain and the volume fraction of each morphology are averaged in each β grain and then in the whole representative volume.

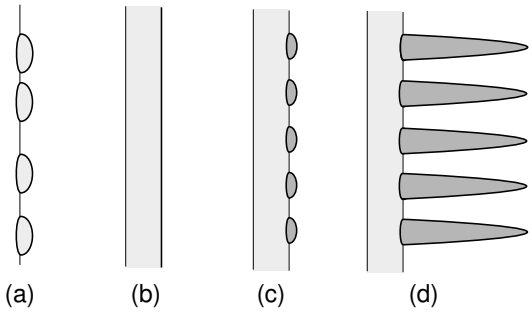

Fig. 2. Sequence of the phase transformation modelling for the high temperature morphologies: (a) nucleation of α_{GB}, (b) growth of α_{GB}, (c) appearance of α_{WGB}, and (d) growth of α_{WGB} [3].

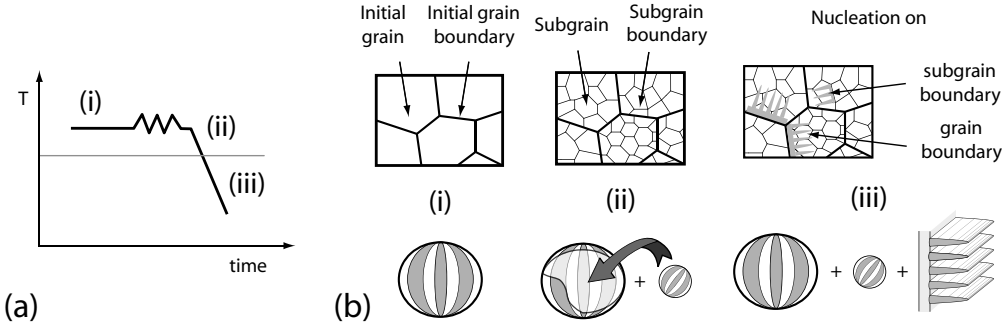

Fig. 3. (a) The different stages of the thermo-mechanical process; and (b) the associated microstructural evolutions with their geometrical simplifications.

2.1.2 Deformed microstructure

During plastic deformation, recovery and Continuous Dynamic Recrystallisation (CDR) of the β phase occur, generating small subgrains (subGBs) inside the initial grains [1,10–15], as explained in detail in [16]. The subGBs have almost the same size ($\approx 10\ \mu$m diameter) and are also represented by equivalent spheres (Fig. 3). Their boundaries are low-angle as well as high-angle GBs. The number of subgrains depends on the deformation rate, when the misorientation of the boundaries/sub-boundaries depends on the deformation amount.

According to the observations on the β-Cez alloy [1,2] and to former studies on other titanium alloys [17,18], it is established that the new grain and subgrain boundaries generated by the CDR must be accounted for as nucleation sites as discussed below.

Moreover, despite some microstructural observations [1,10], it is not completely clear if the new boundaries are obstacles to the growth of the α_{WGB} plates. Hence, geometrical assumptions corresponding to the two limit cases are considered in this study:
(i) all the boundaries (GBs and subGBs) stop the α_{WGB} plates. The calculation is performed as described above by simply replacing D_{gr} by D_{sub}, the diameter of the subgrains.
(ii) The subgrain boundaries can be crossed by α_{WGB}, and the only obstacles are the GBs of the large initial β grains. In order to account for the new boundaries, the number of faces of each initial β grain is increased as following:

$$N_{\mathrm{face}} = 14\,(D_{\mathrm{gr}}/D_{\mathrm{sub}})^3 \tag{1}$$

with surface:

$$S_{\mathrm{face}} = \pi\, D_{\mathrm{sub}}^2/14 \tag{2}$$

Eqs. (1-2) assume that the new boundaries are distributed homogeneously inside the initial β grains. The calculations will then have to be considered with care, because the new boundaries have been observed to appear preferentially in the vicinity of the initial GBs, leaving the core of the initial β grains almost unchanged. However, this spatial heterogeneity of the substructure is observed only for small plastic strains [1].
Another effect which could be accounted for is the geometrical recrystallisation. It consists in the flattening/stretching of the initial β grains by the macroscopic strain, increasing their specific GB surface [1]. Conversely to other studies [4,19,20], this effect is assumed negligible when compared to the generation of new subGBs as justified in [21].

2.2 Nucleation and growth of α_{GB}

A prior plastic deformation of β increases the nucleation rate of α_{GB} at the boundaries as clearly shown by [1,2]. In the present study, it is assumed that this is due to the increase of the misorientation angles of all the GBs by the CDR [1,16]. Consequently, their potential for heterogeneous nucleation increases with their energies. In our model, these processes are described by the time t_n necessary for α_{GB} to cover the surface of the GB where they have nucleated [3]. Following [21], t_n is simply $t_n \approx 1/J^*$, where J^* is the nucleation rate. A pillbox geometry has been used for the α_{GB} nuclei, following [22,23]. J^* can be expressed with the classical theory of heterogeneous nucleation [24]:

$$J^* = \frac{2\nu_{\mathrm{at}}\sqrt{\epsilon}D_{\mathrm{min}}x_{\mathrm{min}}^{\beta}}{a^4\sqrt{3k_{\mathrm{B}}T}}\exp\left(-\frac{4\pi\chi\gamma_b^2}{\Delta G_v^2 k_{\mathrm{B}}T}\right) \tag{3}$$

with $\chi = 2\,\gamma_{\alpha\beta} - \gamma_{\beta\beta}$, $\gamma_{\beta\beta}$ the grain or subgrain boundary energy, $\gamma_{\alpha\beta}$ the interfacial α/β energy at the upper face of the pillbox and γ_b at its edge. The other terms are defined in [24] following their classical meaning found in any textbook.

In Eq. (3) the influence of the prior plastic deformation of β is accounted for by $\gamma_{\beta\beta}$, which is calculated from the misorientation angle θ of the boundaries. Indeed, there is no direct measurement of $\gamma_{\beta\beta}$ available for these alloys, whereas distributions of the θ values have been determined experimentally for a large range of plastic deformation conditions [1]. These distributions are hence input data of the model: for each face inside the representative volume, a value of $\gamma_{\beta\beta}$ is calculated from these distributions using the empirical relation proposed by Wolf, valid on the whole range of GB angles [25]:

$$\gamma_{\beta\beta} = \gamma_0 \sin\theta\,[A - \ln(\sin\theta)] \tag{4}$$

where $A = 4\pi(1-\nu)\,k$, $\gamma_0 = \mu\,b/[4\pi(1-\nu)]$, μ is the shear modulus, ν the Poisson ratio, b the modulus of the Burgers vector, and $k = E_{\text{core}}/(\mu\,b^2)$ with E_{core} the core energy of the dislocations.

Since there is no measurement of $\gamma_{\alpha\beta}$ and γ_b, their values have been adjusted as described in the next section. The same value of γ_b have been set to all the faces, whereas the values of $\gamma_{\alpha\beta}$ are distributed following a normal law to account for the many parameters which can play a role in the nucleation process. Indeed, vacancies and dislocations can enhance the nucleation rate by either decreasing the energy barrier or enhancing diffusion [5,19,26]. Morevover, the β grain misorientation influences the shape and size of the critical α_{GB} precipitates [17,27–29], and thus the nucleation rate J^*. Finally, the elastic energy stored near the grain boundaries during plastic deformation arising from the strain incompatibility between the grains depends on the grain misorientation [30]. Distributing the values of $\gamma_{\alpha\beta}$ is a crude but simple approach to include all these effects, because of the lack of accurate models.

According to some observations in the β-Cez alloy [2], the growth rate of α_{GB} is almost not affected by a prior plastic deformation. Similar observations have been made for the case of steels [4,5]. Thus the approach followed in [3], for the case of non deformed microstructures, can be adopted here. The growth of α_{GB} is assumed to be planar and controlled by the diffusion of the partitioning species. Assuming that the β phase is an ideal solution, the equilibrium at the α/β interface is described by a solubility product. Moreover, the β grain is assumed to be an infinite medium. This is reasonable for this morphology because the order of magnitude of the diffusion lengths in front of α_{GB} is much smaller than the size of the β grains.

2.3 Appearance and growth of α_{WGB}

The appearance of α_{WGB} and its coupling with a prior plastic deformation are issues which have not been much studied. The morphological destabilization of α_{GB} has been proposed on the basis of EDX measurements by [31]. Other studies such as [29] have suggested that the α_{WGB} plates appear by the sympathetic nucleation of α on the α_{GB} layers. Recent observations of Widmanstätten ferrite in a low carbon steel [32] confirm the possibility of this last mechanism. Nevertheless, more experimental studies are necessary to place the modeling on a firmer footing. Therefore, the empirical approach proposed in [3] is followed in this study. At each face, one α_{WGB} colony appears when a α_{GB} layer has reached a critical width W_c. In [3], W_c was chosen equal to the measurements W_c^0 by [2] in the β-Cez alloy for a non-deformed microstructure, i.e. for high GB angles. However, W_c is likely to depend strongly on the misorientation angles θ of the boundaries. Indeed, there are many experimental evidences that the shape of the allotriomorph precipitates is correlated to the GB misorientation in different alloys: in Ag-Al [38], Al-Cu [33], Al-Zn-Mg [34,35], as well as in titanium alloys [17,28,36]. In particular, it is observed that the matching between the boundary plane and the habit plane of the precipitates would be the determining factor for nucleation. Considerations on the elastic energy to overcome during the nucleation of new precipitates [37] support these observations. However, most of these studies about the variant selection on the different grain boundaries (high angle, low angle and twin) do not give a clear picture of the trend that has been observed by [1]: "primary" sideplates are observed to grow directly from low angle GBs, when allotriomorphs are observed to grow prior to the "secondary" sideplates on high angle GBs. Similar observations were reported on by [18]. To give some clue to this tendency, Fig. 4 shows an orientation map obtained by electron back-scattered diffraction (EBSD) analysis of a near-β titanium alloy specimen. This specimen has been solution treated in the β phase field for 5 min., then quenched down to 800 $^\circ$C and hold at this temperature until complete transformation. The orientation map was acquired in a SEM-FEG Philips XL 30 with a step size of 1 μm. Each measurement point is colored according to the color keys given with standard triangles, one for each phase. Small variations in the color of a same phase correspond to small misorientations. Most of the high angle GBs are occupied by α_{GB} layers. The particular α_{WGB} colony surrounded with a black line and labelled "A" has appeared directly at a subGB with a misorientation of 7 $^\circ$ separating two subgrains labelled respectively "I" and "II" (in light and dark pink), and has grown into subgrain I.

Of course, more experimental work is needed to lend support to these qualitative observations. Hence, at a first step, we have tested two empirical approaches.

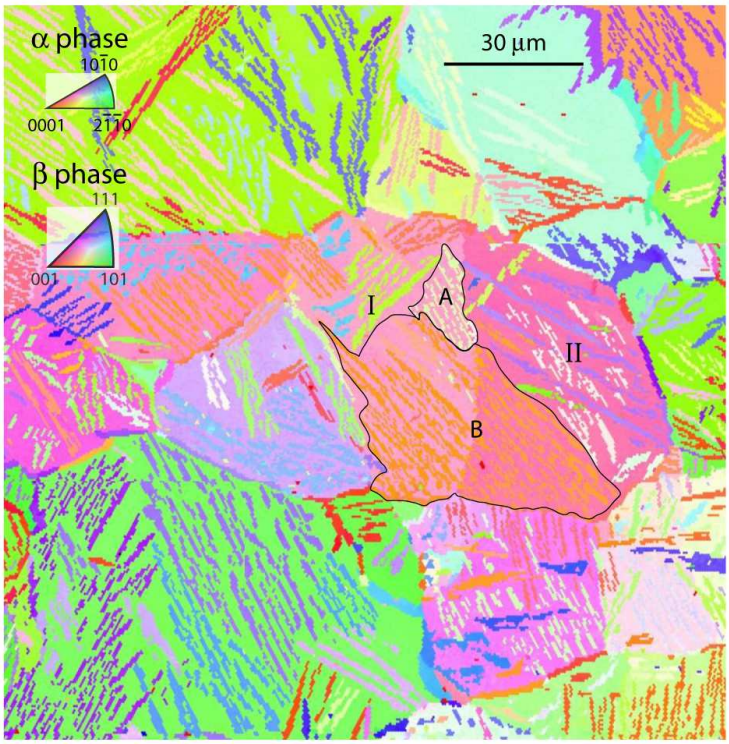

Fig. 4. Orientation map of a near β titanium alloy, solution treated in the β phase field, and hold at 800 $^\circ$C until complete transformation.

In the first one, one α_{WGB} colony appears when the α_{GB} layer width has reached W_c^0, independently of the misorientation angles. In the second one, the critical width of α_{GB} is corrected such that the α_{WGB} colonies appear more rapidly at low angle GBs:

$$W_c = \frac{\gamma_{\beta\beta}}{\gamma^0_{\beta\beta}} W_c^0 \tag{5}$$

with $\gamma^0_{\beta\beta}$ the maximum energy of high angle GBs corresponding to $\theta = 90^\circ$ in Eq. (4).

As for the α_{GB} morphology, the growth of the α_{WGB} colonies is not affected by a prior plastic deformation [2,4,5]. The same approach as in [3] is taken to calculate their growth rate and the main hypothesis are recalled here. The plates are assumed to be parabolic cylinders which grow by a diffusion controlled process. The growth model relies on solving the conservation equations for each partitioning species in the β matrix and assuming the local equilibrium at the interface, with the accounting of the curvature of the plate tip. The β matrix is considered as an infinite medium, for the same reasons put forward for α_{GB}: the characteristic lengths of diffusion in front of the colonies are very small compared to the β grain size. The hard impingement of the α_{WGB} colonies is treated in a simplified way. Inside each β grain or sub-grain,

the length of the colonies increases while the grain is not filled by them. That means that the length of the colony may go beyond the diameter of the grain. In practise, we verified that this happens very rarely and that the lengths averaged in the 100 β grains are always largely inferior to the grain diameter. Finally, Fig. 4 supports the assumption that α_{WGB} can cross subGBs. Indeed, the colony labelled "B" clearly crosses the subGB with the misorientation of 7 $^\circ$, between subgrains I and II. Similar observations were done in [1] on a greater number of specimens. Moreover, from an optical micrograph of a specimen with 0.25 of deformation at a rate of 10^{-1} s^{-1}, the longest of the α_{WGB} colonies can be estimated at about 70 μm, a size far greater than the average subgrain size obtained in these conditions (Tab. 1). Provided that the distribution of the sizes is narrow around its mean value as observed in [1], this would mean that the longest colonies are likely to have crossed subGBs, in agreement with Fig. 4.

3 Results

3.1 Data and parameters

The elastic constants of the β phase are necessary to use Wolf's relationship. According to Ogi [43], the Young modulus and Poisson coefficient are respectively $E = 58$ GPa and $\nu = 0.4$ for pure polycrystalline titanium at 1000 $^\circ$C. The value of k in Eq. (4) is unknown. It has been set such that Eq. (4) gives the energy of a real high angle GB for $\theta > 15^\circ$. According to some measurements in pure titanium, TA6V [44], and Ti-5Al-2.5Sn [45], $\gamma_{\beta\beta}$ ranges between 550 and 850 mJ/m^2, corresponding to values of k between 0.1 and 0.15. This range is consistent with the values found in other metals such as nickel ($k = 0.17$) [46], or tantalum ($k = 0.16$) [47]. In this study, a value of 0.12 has been chosen, corresponding to a high angle GB energy of 800 mJ/m^2. Values of $\gamma_{\alpha\beta}$ and γ_{b} are also necessary for calculating the nucleation rate. There is unfortunately no direct measurement available. Usually, these parameters are adjusted on the basis of measurements of nucleation rates [22,23,48]. Due to the lack of such measurements for our alloy, these parameters have been adjusted such that the calculated overall transformation kinetics fit the measurements for isothermal treatments without any prior deformation. Two different alloys have been considered to enlarge the data set used for the adjustement (β-Cez alloy [2], and Ti17 alloy [21]) between 750 and 830 $^\circ$C. Because this temperature range is narrow, it is assumed that the interfacial energies do not depend on the temperature. We have found $\gamma_{\mathrm{b}} = 20$ mJ/m^2, the average value $\langle\gamma_{\alpha\beta}\rangle = 400$ mJ/m^2, and the standard deviation $\delta\gamma_{\alpha\beta} = 160$ mJ/m^2 (i.e. 90% of the values are between 140 and 660 mJ/m^2).

3.2 Growth of the α_{WGB} colonies inside the deformed β microstructure

First, we have determined whether or not the new boundaries resulting from the CDR must be considered as obstacles to the growth of α_{WGB} colonies. In order to assess the two limit cases presented above, a β microstructure deformed at the rate $\dot{\varepsilon} = 0.1\ s^{-1}$ to the total strain $\varepsilon = 0.25$, containing a large specific surface of subGBs, is considered, with features reported in Tab. 1 [1].

Deformation rate (s^{-1})		Non deformed	10^{-3}	10^{-2}	10^{-1}
Sub-grain or grain diameter (μm)		130	60	20	12
Available specific surface (10^4 m^{-1})		4.6	10	30	50
$0 < \theta < 15\,^\circ$	$0 < \gamma_{\beta\beta} < 510$ mJ/m^2	15%	54%	70%	87%
$15 < \theta < 30\,^\circ$	$510 < \gamma_{\beta\beta} < 700$ mJ/m^2	15%	14%	10%	10%
$\theta > 30\,^\circ$	$\gamma_{\beta\beta} > 700$ mJ/m^2	70%	32%	20%	3%

Table 1
Parameters used to describe the β microstructures resulting from a solution treatment in the β field for 20 min. followed by a plastic deformation at the same temperature with $\varepsilon = 0.25$ at different strain rates [2].

Deformation rate (s^{-1})	Non deformed	10^{-3}	10^{-2}	10^{-1}
Final specific wetted surface (10^4 m^{-1})	2.0	2.6	4.0	5.8
Proportion of activated nucleation sites	44%	26%	13%	12%

Table 2
Results for the β microstructures of Tab. 1 after an isothermal treatment at 800 $^\circ$C.

Calculations have first been performed assuming that all the new boundaries can stop the growth of α_{WGB}. The transformed volume fraction ξ is plotted versus time in Fig. 5, for an isothermal treatment at 800 $^\circ$C. As explained in detail in [3], its evolution can be split into 4 stages. The duration of the nucleation step is about 100 s. The parabolic growth of α_{GB} is then predicted bewteen 100 s and 1000 s, followed by the growth of α_{WGB}. After 1500 s, the transformation rate begins to decrease, when more and more sub-grains are filled. Finally, ξ reaches the maximum value of 0.81, far below equilibrium. Indeed, there is no transformation in about 19% of the subgrains. This quite unexpected result has two reasons.
(i) The untransformed subgrains have mainly low angle boundaries where the nucleation is more difficult. Indeed, as explained in [3] and [21], nucleation occurs very quickly when $\gamma_{\beta\beta} > 2\gamma_{\alpha\beta}$; on the contrary, when $\gamma_{\beta\beta} < 2\gamma_{\alpha\beta}$, the nucleation step is much longer than the duration of an isothermal treatment. As a result, the wetted specific surface correlated to the proportion of activated

nucleation sites is small as shown in Tab. 2.
(ii) It has been assumed that all the sub-boundaries are obstacles to the growth of the α_{WGB} colonies. Without this assumption, α_{WGB} colonies which originate from adjoining subgrains could cross the boundaries of the untransformed subgrains and fill them.

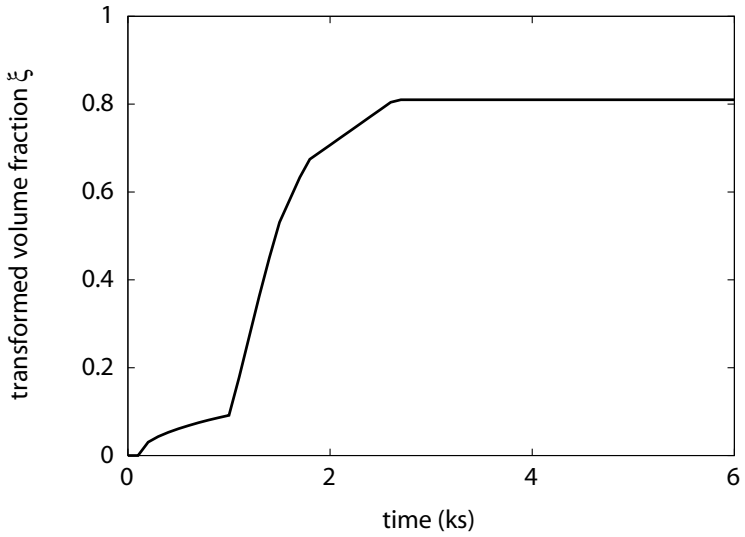

Fig. 5. Transformed volume fraction ξ versus time for an isothermal treatment at 800 $^\circ$C, assuming "impervious" sub-grains.

Then, in order to study the second limit case (i.e. crossing of the subGBs by α_{WGB}), the initial β microstructure is modelled geometrically as one large β grain containing as many faces as there are GBs and subGBs. The respective diameters of the β grains and subgrains are 130 and 12 μm respectively (Tab. 1). According to Eq. 1, the total number of faces is 17800, which is large enough so that only one grain can be statistically representative of the deformed microstructure. ξ versus time is plotted in Fig. 6 for a treatement at 800 $^\circ$C. Contrary to the first limit case, ξ reaches equilibrium. For 1500 s, the two cases are identical because the wetted surface per unit volume is the same. After 1500 s, ξ increases linearly to 1 because the colonies are not stopped by the subGBs. Indeed, the α_{WGB} growth rate is constant for a given temperature, and soft impingement is neglected in the model [3].
This second limit case appears to be more realistic than the first one, because the equilibrium volume fraction of α is reached. Consequently, all the further calculations are performed with this assumption.

3.3 Appearance of α_{WGB} on the sub-grain boundaries

The previous results have been compared with experimental results [1] in Fig. 7a. These calculations were performed assuming that the maximum width of α_{GB} is W_c^0 for all the misorientation angles. The total duration is quite well

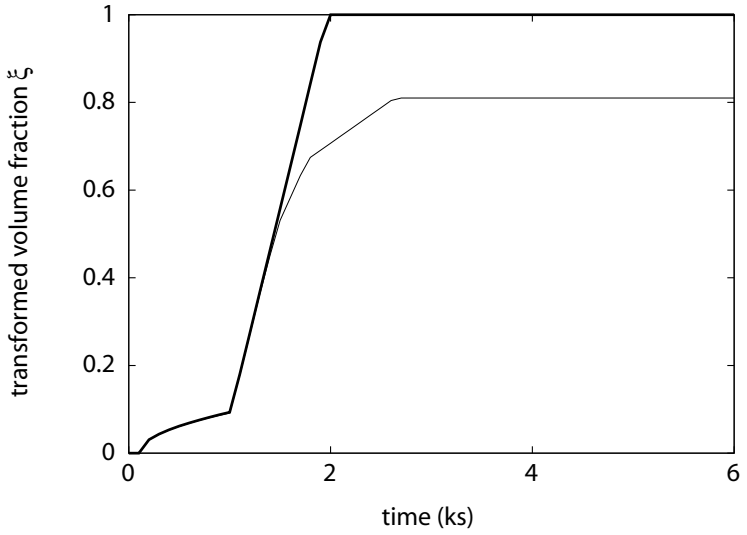

Fig. 6. Transformed volume fraction ξ versus time for an isothermal treatment at 800 °C, assuming sub-grains "impervious" (thin line) or not (thick line) to the growth of α_{WGB}.

estimated: the time necessary to reach $\xi = 0.9$ is only 300 s later than the experiment. Moreover, the slope of the curve during the α_{WGB} growth stage is in fair agreement with the experiments. A good agreement is also found for the number of α_{WGB} colonies per unit volume, supporting the calculation of the GBs surface available for the nucleation of α (Tab. 1).
However, it can be noticed that the transformation rate is largely underestimated during the first stage, with an unobserved sharp transition from α_{GB} to α_{WGB} at about 1000 s. This sharp transition comes from the assumption that all the α_{WGB} colonies appear when the α_{GB} width has reached the same value W_c^0 whatever the considered face. Indeed, the distribution of the nucleation durations t_n is sharp. As a consequence, all the α_{GB} layers reach the critical width W_c^0 at almost the same time, corresponding to the transition from α_{GB} to α_{WGB}.
The overestimation of the duration of the α_{GB} growth stage can also be explained by the nucleation stage. Indeed, the hypothesis of an underestimated parabolic growth rate can be dismissed, when examining the results obtained for the non-deformed case (Fig. 7b). In this last case, there are mostly high angle GBs for which the average α_{GB} width has been determined experimentally to be W_c^0 [2]. On the contrary for the deformed microstructure, two thirds of the wetted surface belongs to low angle GBs resulting from the CDR (Tabs. 1-2). The α_{GB} widths have never been measured systematically on these subGBs, and the available SEM micrographs do not even show a significant precipitation of α_{GB} on these sites. Hence, due to the lack of accurate observations, the critical width of α_{GB} has been corrected with Eq. 5, accounting for a link between the misorientation angle and the transformation sequence.

The calculation accounting for this correction is compared to the experiment

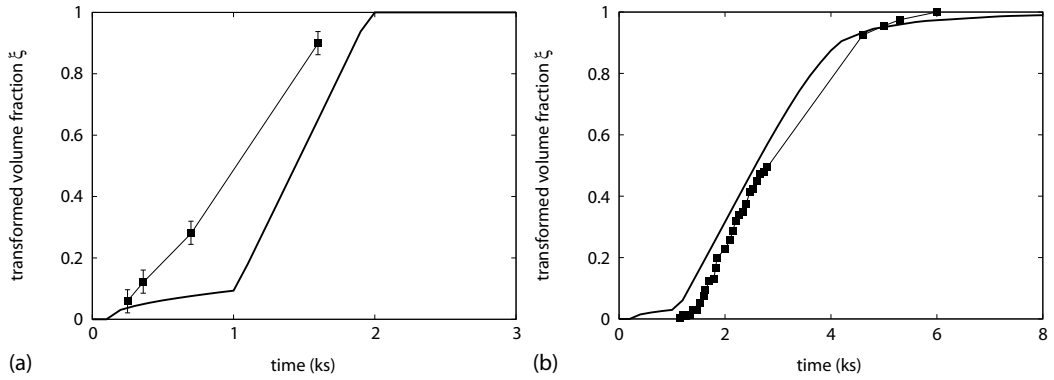

Fig. 7. Transformed volume fraction ξ versus time for an isothermal treatment at 800 $^\circ$C (calculations in continuous lines and experiments with dots): (a) deformed (experiments from [1]) and (b) undeformed β microstructure (experiments from [2]).

in Fig. 8a. It is very close to the experiment for the α_{WGB} growth stage as well as for the beginning of the transformation. Instead of the former sharp transition from α_{GB} to α_{WGB}, the growth rate increases smoothly. Indeed, the α_{GB} layers do not reach W_c at the same time. This is confirmed in Fig. 8b: the number of α_{WGB} colonies per initial β grain is plotted versus time along with the result without correction. It can be noticed that the final number of α_{WGB} colonies is the same with and without correction because the nucleation rate is the same in both case. For the non deformed β microstructure, the correction of W_c has negligible consequences because the distribution of the GB misorientation angles is narrow (Tab. 1): the distribution of the critical widths is thus also narrow.

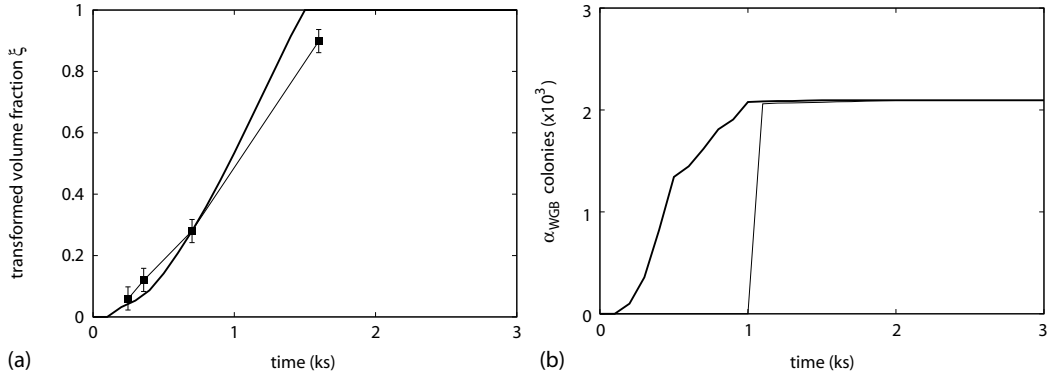

Fig. 8. Isothermal treatment at 800 $^\circ$C: (a) calculated ξ versus time with corrected W_c (continuous line) compared with measurements (dots); (b) number of colonies per initial β grain, with (thick) and without correction (thin).

3.4 Influence of the sub-grain size

The influence of the sub-grain size on the transformation rate has been assessed by considering 3 different β microstructures deformed to the total strain $\varepsilon =$

0.25. Their respective sub-grain sizes have been controlled by the strain rate $\dot{\varepsilon}$ (Tab. 1) [1].

In Fig. 9a, ξ versus time is plotted for the 3 deformation rates during an isothermal treatment at 800 °C. The non deformed case is also shown for comparison. As expected, all the deformed β microstructures undergo quicker transformations than the non deformed one. Indeed, a decrease of the sub-grain size induces an acceleration of the transformation beginning, as well as an increase of the overall transformation rate. In order to explain these features, the specific wetted surface is plotted versus time in Fig. 9b and reported in Tab. 2, because it is directly related to the area per unit volume of the faces where α_{WGB} is growing.
The beginning of the transformation is quicker when the sub-grain size is smaller: there are more low angle GBs where α_{GB} reaches its critical size more quickly to give fast growing α_{WGB} colonies. The increase of the overall transformation rate results from a greater final specific wetted surface (Tab. 2). It can be noted that the wetted surface stops increasing at the same time for all the cases, when the α_{GB} layers at the most misoriented GBs reach W_c^0
It is important to note that inside all the deformed β microstructures, the proportions of activated nucleation sites are very close to each others (Tab. 4). Therefore, the increase in the overall transformation rate is linked to the subGB size and not to the misorientation angle distributions.

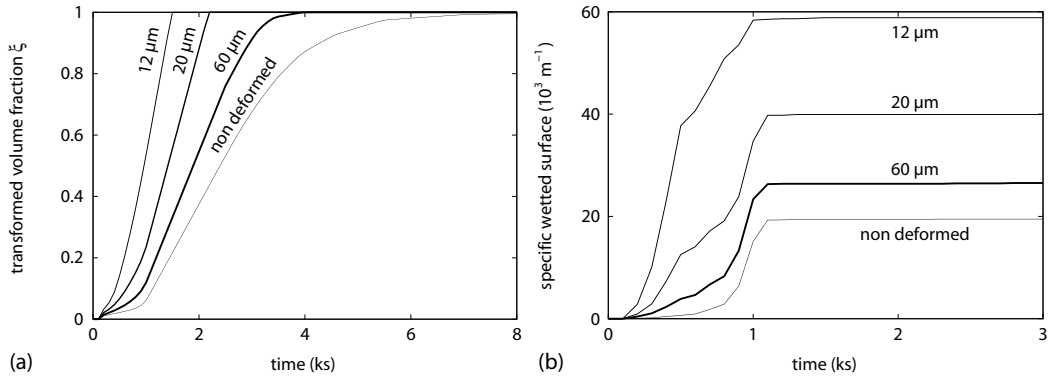

Fig. 9. Isothermal treatment at 800 °C: influence of the sub-grain diameter. (a) Transformed volume fraction ξ versus time, for different strain rates; (b) specific wetted surface versus time.

The calculations are compared to experimental transformation kinetics [1] in Fig. 10. For all the sub-grain sizes, the overall agreement is good. This proves the relevance of the sub-grain size as a key parameter for predicting the transformation rate. However, for a sub-grain size of 60 μm (the lower deformation rate), the transformation rate is slightly overestimated. For this particular case, Chaussy [1] had observed that the new subGBs are located near the initial GBs: thus the assumption of an homogeneous layout of the subGBs leads to underestimate the hard impingement of α precipitates growing in the vicinity of initial GBs.

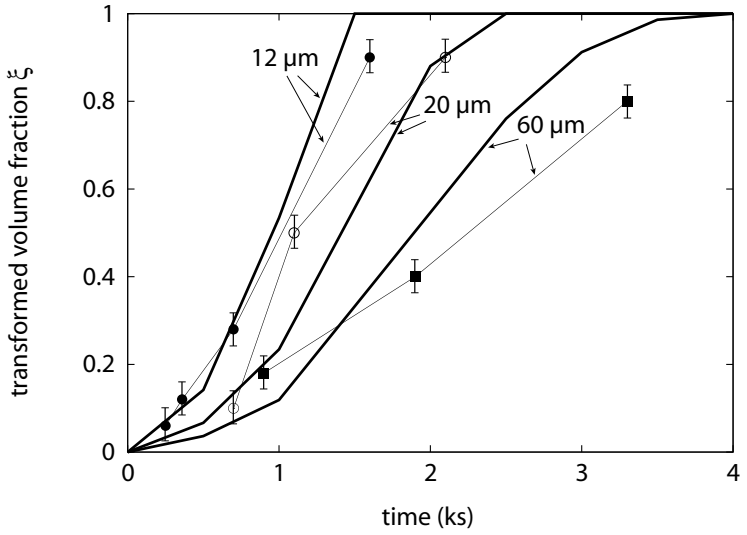

Fig. 10. Isothermal treatment at 800 ° C: transformed volume fraction ξ versus time for different sub-grain diameters (calculations in continuous line and experiments with dots).

So as to further validate our model, we have compared its predictions of some microstructural features with measurements. Because there were no microstrutural measurements available in [1], we have used for that purpose the measurements from [2], on the same alloy which has undergone treatments similar to [1]. Unfortunately, the precise characterization of the misorientation angles distribution was lacking. Nonetheless, a crude estimate on optical micrographs of a specimen deformed at 25% with a rate of 10^{-2} s^{-1} gives an average subgrain size about 60 μm. This corresponds to the specimen of [1] deformed at 25% but with a rate of 10^{-3} s^{-1}. To proceed further, we have thus taken the distribution of the misorientation angles obtained by [1] corresponding to the subgrain size of 60 μm.

A first comparison has been performed in the case of an isothermal treatment at 790 ° C. A fairly good agreement has been achieved for the global kinetics, but a little bit less satisfactory than in Fig. 10: the growth rate during the α_{WGB} stage is slightly underestimated when compared to the measurements. In Fig. 11, we have compared the time evolution of the number of α_{WGB} colonies. We have divided the predicted numbers by 7/3 and 7/4 correponding to the numbers of faces in a tetrakaidecahedron cut by a plane (depending on the orientation), to account for the change from three to two dimensions. 7/4 and 7/3 defines an upper range which is believed to be representative of what is observed on a micrography. As shown in Fig. 11, the agreement is satisfactory between the corrected predictions and the experiments. The slight underestimation of the final number of colonies explains the underestimation of the global kinetics during the α_{WGB} growth stage. These discrepancies may be explained by the uncertainties on the average subgrain size as well as on the distribution of the misorientation angles.

We have performed the same kind of calculations for 750 and 830 ° C, so as to compare the variation of the width of α_{GB} with the temperature. Indeed, it has been observed by [2] that there is a very small dependence of the average α_{GB} upon the deformation, as shown in Fig. 12 (black symbols), whatever the temperature. A very good agreement is achieved between the experiments and the calculations, which are quite insensitive to moderate variations of the average subgrain size.

These results tend all to confirm the validity of the assumptions of our model.

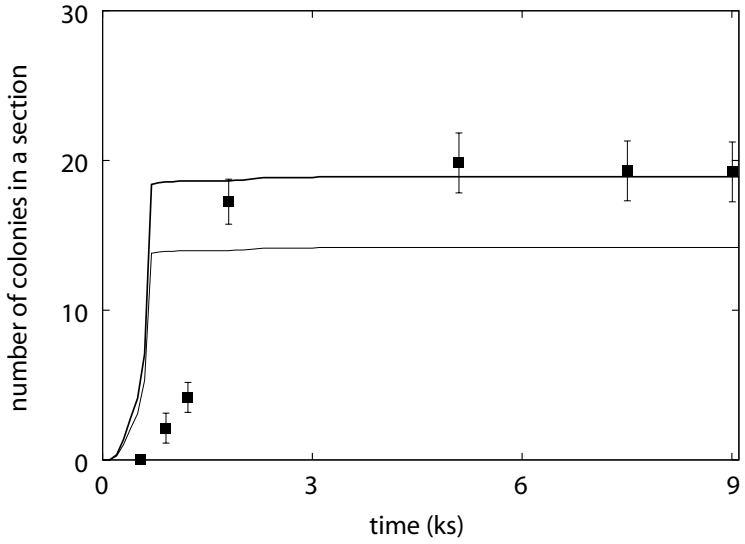

Fig. 11. Isothermal treatment at 790 ° C of a specimen deformed of 25% at 10^{-2} s^{-1}: time evolution of the number of colonies in a 2D section (calculations in continuous line and experiments with dots).

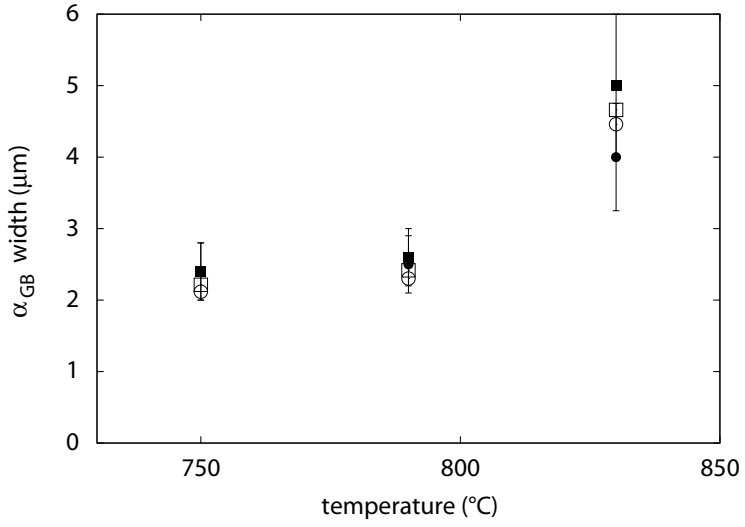

Fig. 12. Average α_{GB} width versus temperature for non deformed specimens (squares) and specimens deformed of 25% at 10^{-2} s^{-1} (circles); calculations are with white symbols and experiments with black ones.

3.5 Influence of the boundaries misorientation

The influence of the distribution of misorientation angles has been studied by considering different deformed β microstructures with features appearing in Tab. 3. They all have the same sub-grain size of 12 μm (associated with a same deformation rate), but different distributions of the misorientation angles with the average value increasing with the plastic deformation.

Plastic deformation		Non deformed	0.25	0.75	1	1.5
Sub-grain or grain diameter (μm)		130	12	12	12	12
Available specific surface (10^4 m^{-1})		4.6	50	50	50	50
$0 < \theta < 15^\circ$	$0 < \gamma_{\beta\beta} < 510$ mJ/m^2	15%	87%	70%	63%	63%
$15 < \theta < 30^\circ$	$510 < \gamma_{\beta\beta} < 700$ mJ/m^2	15%	10%	13%	15%	13%
$\theta > 30^\circ$	$\gamma_{\beta\beta} > 700$ mJ/m^2	70%	3%	17%	22%	22%

Table 3
Parameters used to describe the β microstructures resulting from a solution treatment in the β field for 20 min. followed by a plastic deformation at the same temperature with the same strain rate but with different total strains [1].

Plastic deformation	Non deformed	0.25	0.75	1	1.5
Final specific wetted surface (10^4 m^{-1})	2.0	5.9	9.1	10.2	10
Proportion of activated nucleation sites	44%	12%	18%	20%	21%

Table 4
Results for the β microstructures of Tab. 3 after an isothermal treatment at 800 $^\circ$C.

In Fig. 13, the calculations for the different plastic deformations are plotted in the case of an isothermal treatment at 800 $^\circ$C. As expected, the lowest prior plastic strain $\varepsilon = 0.25$ leads to the slowest beginning and to the lowest overall transformation rate. For higher plastic deformations, the transformation kinetics are surprisingly almost identical. In fact, the lowest overall transformation rate results from the lowest wetted specific surface. On the other hand, the almost identical transformation rates for $\varepsilon \geq 0.75$ result from very close specific wetted surfaces (Tab. 4).

The calculations are compared to experimental results [1] in Fig. 14. In all cases, the calculated durations of the transformation are in good agreement with the measurements, showing that the wetted GB surface by α is well assessed. Moreover, the evolution of the average slope with respect to the strain is in agreement with the experimental observations: $\varepsilon = 0.25$ has the smaller slope, whereas the higher strains have a greater slope, almost the same. These trends are consistent with the calculated specific GB surfaces wetted

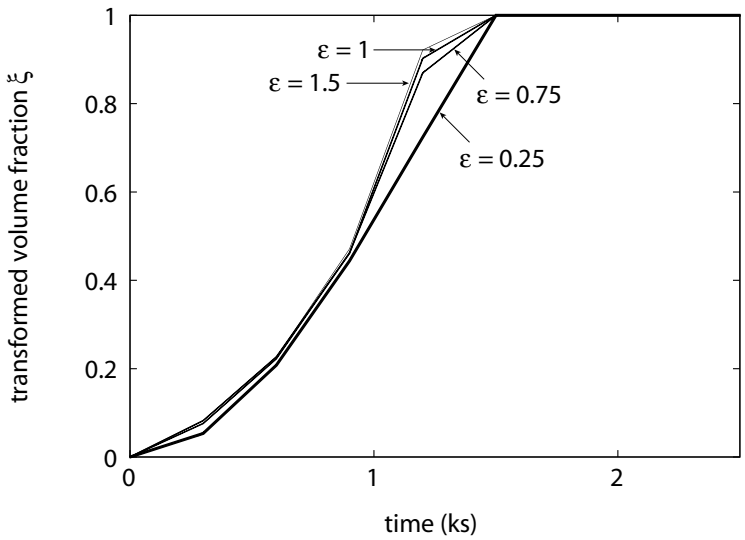

Fig. 13. Isothermal treatment at 800 °C. Calculated transformed volume fraction ξ versus time, for different plastic strains.

by α (Tab. 4). These results hence support the relevance of the misorientation angles as parameters for describing the deformed β microstructure.

However, the calculations do not predict the continuous shift of the beginning of the transformation when the plastic strain increases, as observed in experiments: a more accurate modeling of the transformation at the beginning is necessary. Indeed, on one hand it should be necessary to further analyze our hypothesis of a stoechiometric α phase, and a possible accelerated diffusion at the GBs (with effect or not of the deformation). On the other hand, the mechanism of appearance of α_{WGB} needs to be studied experimentally in more detail. Moreover, the plastic strain stored in the vicinity of the GBs due to grain incompatibilities is likely to influence the nucleation and growth rates. Indeed, considering the elastic constants of the β phase, a simple assessment of the stored strain energy gives an order of magnitude of 10^6 J/m^3. This value is not negligible when compared to the nucleation driving force, especially at high temperatures, as reported in Tab. 5.

T (°C)	ΔG_v (10^7 J/m^3)
830	1.3
800	2.4
750	4.5

Table 5
Nucleation driving force for the β-Cez alloy.

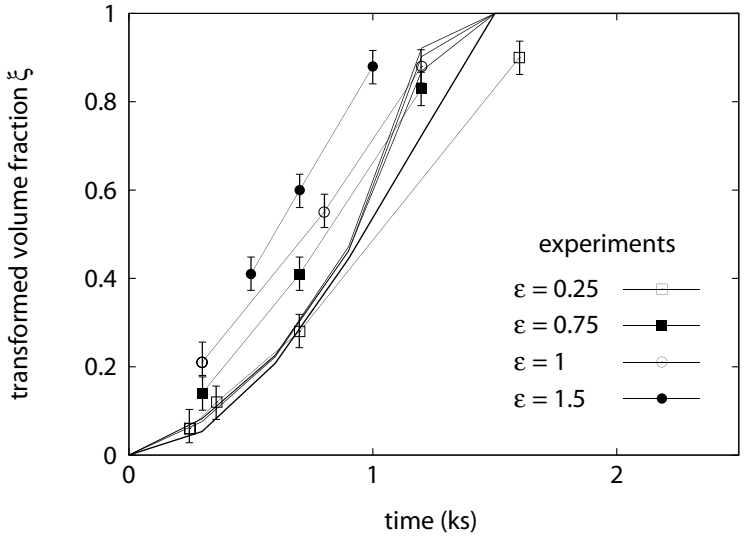

Fig. 14. Isothermal treatment at 800 ° C. Calculated and experimental transformed volume fraction vs. time, for different plastic strains.

4 Conclusion

A model has been developed in order to predict the influence of a prior plastic deformation of the β phase above the transus temperature on the α phase precipitation occurring during a subsequent cooling. The model relies on the explicit calculation of the nucleation and growth rates of the precipitates, as developed in [3]. Two major improvements has been carried out to this model in the present study: first, a suitable geometrical representation of the microstructure is proposed where subGBs are additional nucleation sites for the α_{GB} allotriomorphs. Second, the calculation of the nucleation rate at the GBs is now dependent on the plastic deformation conditions, through the distributions of the misorientation angles.

Preliminary calculations have been performed to assess the relevance of some assumptions related to the appearance and growth of the α_{WGB} colonies: the α_{WGB} colonies are hence likely to cross the subGBs; and the critical width of the α_{GB} layers controlling the transition to α_{WGB} must decrease with decreasing misorientations for the calculated kinetics to match the measurements. Of course, additional experimental work is required to confirm these conclusions.

Finally, calculations have been compared to experiments for initial deformed β microstructures with different conditions. A very good agreement has been achieved concerning the influence of the strain rate changing mainly the subgrain size: the faster the strain rate, the smaller the subgrain size and the faster the transformation. The agreement is fair concerning the influence of the strain which changes dramatically the distribution of the misorientation angles. The tranformation rate during the α_{WGB} growth stage saturates at higher strain as observed. Unfortunately, the model is unable to describe the influence of the strain on the first stage of the transformation, involving the nucleation of the

allotriomorphs as well as the transition to the Widmanstätten colonies. More experiments are obviously needed to understand the involved mechanisms and their link to a prior plastic deformation. Nonetheless, a better analysis of the formation of α allotriomorphs, which would account for the strain stored in the vicinity of the GBs, has been suspected to be an essential ingredient for describing quantitatively this effect.

5 Acknowledgment

Snecma is gratefully acknowledged for the financial support of this work.

References

[1] Chaussy F. PhD thesis, INPG, Grenoble; 1996.

[2] Laude E. PhD thesis, INPL, Nancy; 1997.

[3] Appolaire B, Hericher L, Aeby-Gautier E. Acta Mater 2005;53:3001.

[4] Umemoto M, Ohtsuka H, Tamura I. Trans ISIJ 1983;23.

[5] Umemoto M, Hiramatsu A, Moriya A, Watanabe T, Nanba S, Nakajima N, Anan G, Higo Y. ISIJ Int 1992;32,306.

[6] Gautier E. PhD thesis, INPL, Nancy; 1985.

[7] Lee CH, Bhadeshia HKDH, Lee HC. Mat Sci Eng A 2003;360:249.

[8] Larn RH, Yang JR. Mat Sci Eng A 1999;264:139.

[9] Larn RH, Yang JR. Mat Sci Eng A 2000;278:278.

[10] Chaussy G, Driver JH. Revue de Métallurgie, CIT, 1996;93:1057.

[11] Chaussy F, Driver JH. In: Vassel A, Eylon D, Combres Y, editors. Les alliages de titane beta. SF2M, Editions de la Revue de Métallurgie; 1994;8:57.

[12] Balasubrahmanyam VV, Prasad YVRK, Mat Sci Eng A 2002;336:150.

[13] Philippart I, Rack HJ, Mat Sci Eng A 1998;254:253.

[14] Furuhara T, Toji Y, Maki T. In: Ltjering G, Albrecht J, editors. Proceedings of the 10^{th} World Conference on Titanium. Hamburg, Germany: DGM; 2003. p. 1219.

[15] Furuhara T, Toji Y, Abe H, Maki T, Mat Sci Forum 2003;426-432:655.

[16] Gourdet S, Montheillet F. Acta Mater 2003;51:2685.

[17] Furuhara T, Maki T. Mat Sci Eng A 2001;312:145.

[18] Aaron HB, Aaronson HI. Metall Trans 1971;2:23.

[19] Hanlon DN, Sietsma J, van der Zwaag S, ISIJ Int 2001;41:1028.

[20] Lacroix S, Bréchet Y, Véron M, Quidort D, Kandel M, Iung T, Symposium on the Thermodynamics, Kinetics, Characterization and Modeling of Austenite Formation and Decomposition, Chicago, Illinois, 9-12 Nov. 2003, pp. 367-379, 2003.

[21] Da Costa Teixeira J. PhD thesis, INPL, Nancy; 2005.

[22] Menon ESK, Aaronson HI, Metall Trans A 1986;17:1703.

[23] Plichta MR, Perepezko JH, Aaronson HI, Lange III WF. Acta Mater 1980;28:1031.

[24] Russell KC, Acta Metall 1969;17:1123.

[25] Wolf D, Scripta Mater 1989;23:1713.

[26] Liu J, Yanagida A, Sugiyama S, Yanagimoto J. ISIJ Int 2001;41:1510.

[27] Gheorge M, Qazi JI, Rack HJ. In: Lütjering G, Albrecht J, editors. Proceedings of the 10th World Conference on Titanium. Hamburg, Germany: DGM; 2003. p. 1155.

[28] Miyano N, Fujiwara H, Ameyama K, Weatherly GC. Mat Sci Eng A 2002;333:85.

[29] Furuhara T, Takagi S, Watanabe H, Maki T. Metall Trans A 1996;27:1635.

[30] Diligent S, Gautier E, Lemoine X, Berveiller M. Acta Mater 2001;49:4079.

[31] Fujii H, Suzuki HG, 6th World Conference on Titanium. III; Cannes; France; 6-9 Juin 1988. pp. 1489-1494. 1988.

[32] Phelan D, Stanford N, Dippenaar R. Mat Sci Eng A 2005;407:127.

[33] Vaughan D. Acta Met 1968;16:563.

[34] Unwin PNT, Nicholson RB. Acta Met 1969;17:1379.

[35] Park JK, Ardell AJ. Acta Met 1986;34:2399.

[36] Furuhara T, Nakamori H, Maki T. Mat Trans, JIM 1992;33:585.

[37] Simon JP, Guyot P. J Mat Sci 1975;10:1947.

[38] Hawbolt EB, Brown LC. Trans TMS-AIME 1967;239:1916.

[39] Malinov S, Guo Z, Sha W, Wilson A. Metall Mater Trans A 2001;32:879.

[40] Christian JW. Theory of Transformations in Metals and Alloys - Part I, 2nd ed.. London: Pergamon Press; 1975. p. 181.

[41] Angelier C, Bein S, Béchet J. Metall Trans A, 1997;28:2467.

[42] Ahmed T, Rack HJ. Mat Sci Eng A, 1998;243:206.

[43] Ogi H, Kai S, Ledbetter H, Tarumi R, Hirao M, Takashima K. Acta Mater 2004;52:2075.

[44] Roth TA, Suppayak P. Mat Sci Eng 1978;35:187.

[45] Roth TA, Henning WD. Mat Sci Eng 1985;76:187.

[46] Qi Y, Strachan A, Cagin T, Goddard III WA. Mat Sci Eng A 2001;309:156.

[47] Wang G, Strachan A, Cagin T, Goddard III WA. Mat Sci Eng A 2001;309:133.

[48] Veeraraghavan D, Wang P, Vasudevan VK. Acta Mater 2003;51:1721.

[49] Lan YJ, Xiao NM, Li DZ, Li YY, Acta Mater 2005;53:991.